

Preparation and characterization of Spironolactone loaded chitosan – based dry powder: local delivery in pulmonary arterial hypertension via inhalation

AA Yas

Department of Pharmaceutics, College of Pharmacy, Tikrit University, Tikrit–P. O. Box (42), Saladin–Iraq

Abstract: Spironolactone (SL), an aldosterone antagonism being proved by Randomized Aldactone Evaluation Study (RALES) combines with angiotensin converting enzyme (ACE) inhibitors to decrease pulmonary arterial hypertension (PAH) mortality and improve the clinical outcomes. This work represents the employment of a 5^3 central composite design (CCD) for developing a dry powder for inhalation (DPI) containing SL prepared via a sieving method utilizing cross-linked chitosan (CS) with glutaraldehyde (GA) as the carrier. The optimized SL loaded microparticles (OSLM) powder angle of repose (AOR, Y_1), geometric standard diameter (GSD, Y_2), fine particle fraction (FPF, Y_3) and mass median aerodynamic diameter (MMAD, Y_4) responses were optimized after studying the influence of the formulation variables that were CS (X_1), acetic acid (AA, X_2) and GA (X_3). The OSLM was further evaluated on the basis of scanning electron microscopy (SEM), x-ray powder diffraction (XRPD), Fourier transform infrared spectroscopy (FTIR) analysis and drug release kinetic model and mechanism. It was found that Y_1 increase upon X_1 increment only, Y_2 increase rely on X_1 and X_2 combined increment, Y_3 will increase upon X_1 increment up to a certain point after which there will be a decline in the aerosolization performance, whereas Y_4 is more significantly influenced by the X_2 . XRPD reveal that SL existence is in the amorphous state and homogeneously dispersed within the microparticles and the FTIR indicates no physicochemical interaction take place between SL and the carrier. The in vitro release was obeying Korsmeyer-Peppas model, whereas the release mechanism was Fickian diffusion. This approach provides a mean for successful pulmonary delivery of SL in the treatment of PAH.

Keywords: pulmonary arterial hypertension, spironolactone, dry powder inhalation, central composite design, cross-linked chitosan microparticles.

I. Introduction

Pulmonary arterial hypertension (PAH) is a rare disease, with an estimated prevalence ranging from 10-52 cases per million, whereas the 1-year incident survival rates ranging from 68-93% according to countries registries ordered ascending from US NIH registry-PH registry of the UK and Ireland over different time periods [1]. The PAH main feature as a progressive disease is a combination of small pulmonary arteries endothelial dysfunction and increased contractility, endothelial and smooth muscle cells proliferation and remodeling and blood vessels progressive narrowing due to in situ thrombosis. All leads to a progressive blood flow resistance and pulmonary arteries pressures increment [2]. Right ventricular hypertrophy (RVH) developed in order to compensate for the increased after load and cardiac output maintenance, but it is rarely fully compensatory, aggravated into RV ischemia, leads to RV failure and hence shortens lifespan [3].

Recently there is an evidence that the renin-angiotensin-aldosterone system (RAAS) will activate and participate in the PAH pathology, where aldosterone plays a key role in the cardiopulmonary remodeling revealed by its level reduction during angiotensin converting enzyme (ACE) inhibitors administration. The vascular and cardiac cells mineralocorticoid receptors (MR) will be activated by the higher aldosterone levels come from endothelin-1 stimulated extra-adrenal pulmonary aldosterone synthesis, initiate signals that induce vascular remodeling, reduce vascular reactivity and contribute in RV dysfunction which is a prominent PAH cause of death. Spironolactone (SL), an aldosterone antagonism being proved by Randomized Aldactone Evaluation Study (RALES) combines with ACE inhibitors to decrease PAH mortality and improve the clinical outcomes by decreasing muscularized vessels number, increased cross-sectional luminal area, and limited vascular collagen deposition and fibrosis, decreased pulmonary artery systolic pressure and decreased RV hypertrophy [4]. As a combined MR and androgen receptors (AR) antagonist, early stage PAH patients start taking SL has been revealed a treatment novelty by improving endothelial function via its anti-inflammatory effect on the NF κ B-mediated inflammatory signaling in human endothelial cells [5].

Pulmonary drug delivery via inhalation has been employed for the treatment of localized and systemic conditions, and it is clinically acceptable; where in case of localized therapies advantages like needleless route, no hand care required and self administration when patients are properly trained become attractive, whereas in case of systemic therapies, additional features such as large lung peripheral epithelial layer surface area (100

m²), thickness (0.2 – 0.7 μm) and high blood supply that maintain sink condition for drug absorption provoke utilization of the pulmonary route for getting drug rapid onset of action and better permeation [6]. Chitosan (CS) is considered as a physiologically compatible cationic polymer due to biologically non-toxic, mucoadhesive and biodegradable. Chitosan pKa 5.6 make it soluble only in acidic solutions, and then become a polycationic polymer because of the protonated amine groups that imparts high density positive charges, but retains its deprotonated nature at physiological pH in biological fluids [7]. According to the Biopharmaceutical Classification System (BSC); SL considered as a class II drug of low solubility 2.8 mg/100 ml at 25 °C in water and high permeability, then in order to improve its oral bioavailability SL being formulated as nanosuspensions and solid dispersions [8,9].

Involvement of chitosan as a carrier in pulmonary drug delivery when a dry powder inhaler preparation consists of cross-linked CS microparticles with citric acid loaded with cisplatin will improve lung cancer treatment via chemotherapeutic agent targeting besides dose reduction [10], and the same to be achieved with PAH.

Sieving method was the one that utilize in this study for SL-CS microparticles preparation, the formulations were optimized using a 5³ central composite design (CCD) and the optimized formula was physicochemically characterized and pulmonary deposition investigated.

II. Materials and Methods

Materials: Pure spironolactone (SL) was received as a gift sample from the State Company for Drug Industries and Medical Appliances (SDI) (Samarra / Iraq). Chitosan (CS), acetic acid (AA) and glutaraldehyde (GA) were produced from (Himedia-India), (Solvochime-UK) and (Lobachime-India) respectively. All other chemicals/solvents used were of analytical grade.

Preparation of Spirolactone loaded chitosan microparticles by sieving method: A thick jelly mass was produced by dissolving CS into AA solution, SL incorporated into the jelly mass, that became non-sticky upon cross-linked with GA and then the mass passing through a 625-mesh screen sieve (Retsch/Germany) to get a percentage of suitable inhaled sized microparticles. The produced SL loaded CS microparticles were washed with 0.1 N NaOH solution to get rid from excess un-reacted GA and placed in an oven (IMS-Laitram-USA) at 40 °C for an overnight [11].

Experimental design: A single block of 20 conducted experiments was involved and the formulations were determined by a 5³ CCD. The 3 variables that were considered include: CS (X₁), AA (X₂) and GA (X₃). The responses that were considered include: angle of repose (AOR, Y₁), geometric standard diameter (GSD, Y₂), fine particle fraction (FPF, Y₃) and mass median aerodynamic diameter (MMAD, Y₄) of the CS-based dry powder. The Design-Expert Version 8.0.7.1 (Stat-Ease Inc., Minneapolis, MN) was employed for data modeling and statistical analyses.

Statistical data analysis and validity of the optimized model: A multiple linear regression model fitting to a 5³ factorial design yields a predictor polynomial equation that incorporates interactive and polynomial terms to evaluate the responses:

$$Y = b_0 + b_1x_1 + b_2x_2 + b_3x_3 + b_{12}x_1x_2 + b_{23}x_2x_3 + b_{13}x_1x_3 + b_{11}x_1^2 + b_{22}x_2^2 + b_{33}x_3^2 \quad (1)$$

Aims that arise from employing this model is to evaluate the effect of the linear, x_i; quadratic, x_i² and the interactive, x_ix_j, independent variable on the dependent variable. The measured response Y associated with each factor combination; b₀ is an intercept representing the arithmetic average for all quantitative outcomes of the nine runs; b₁ (b₁, b₂, b₃, b₁₂, b₂₃, b₁₃, b₁₁, b₂₂ and b₃₃) are regression coefficients computed from the observed experimental Y values. The five levels for each variable were -1.682, -1, 0, +1, +1.682 and table 1 lists the actual values corresponding to each variable. X₁, x₂ and x₃ are the coded independent variable level.

X₁, x₂ and x₃ are the main effects and after changing one factor at a time the average results. Upon two factors were changed simultaneously the interaction terms show the response. Using a numerical optimization tool via the desirability approach the optimum dependent variables were calculated for the desired response.

Table 1: Central composite design variables					
Factor	Level				
	-1.682	-1	0	+1	+1.682
X ₁ : CS (% w/v)	0.78	1.60	2.80	4.00	4.82
X ₂ : AA (% w/v)	0.35	1.00	1.95	2.90	3.55
X ₃ : GA (% w/v)	0.00	0.25	0.33	0.40	0.45
Response			Constraints		
Y ₁ : angle of repose (AOR, θ)			Minimize		
Y ₂ : geometric standard diameter (GSD, μm)			Minimize		
Y ₃ : fine particle fraction (FPF, %)			Maximize		

Y₄: mass median aerodynamic diameter (MMAD, μm)

Minimize

Dry – powder characterization

Flowability: The funnel method was employed, where an accurately powder weighted amount was taken and allowed to flow freely on the surface, the formed cone diameter was measured and angle of repose (θ) was calculated using equation below^[12]:

$$\theta = \tan^{-1} h/r \quad (2)$$

where, h and r are the height and radius of the powder cone.

Particle size analysis: An optical microscope (Olympus-Japan) fitted with an ocular micrometer and a stage micrometer was employed for geometric particle size distribution measurement and the average particle size of 100 particles from each formula was measured using Edmondson's equation^[13]:

$$D_{\text{mean}} = \Sigma nd / \Sigma n \quad (3)$$

where, n = number of microparticles observed; d = mean size range.

In vitro powder aerodynamics: An eight stage, nonviable Andersen Cascade Impactor (ACI) (Graseby – Andersen / USA) with a preseparator is employed in the FPF determination. Rotahaler[®] was filled manually with 30 mg microparticles from each formula and the ACI was operated at flow of 28.3 l/min for 10 seconds. The ACI effective cut off diameters were 9, 5.8, 4.7, 3.3, 2.1, 1.1, 0.65 and 0.43 μm for stages 0–7, respectively. Definition of the FPF was the fraction of drug less than 5 μm. The microparticles MMAD was determined by plotting inverse cumulative mass percentage against log effective cut off diameter in each stage, whereas GSD obtained from measuring the spread of an aerodynamic particle size distribution^[14].

Particle morphologies: Scanning electron microscope (AIS2300C, Angstrom-USA) was employed for examining SL, CS and the optimized SL loaded microparticles (OSLM) morphologies. Prior microscopy, powder samples were mounted at carbon tape and were sputter-coated using gold (Ion Sputter), then at an acceleration voltage of 20 kV the photomicrographs were taken.

X – ray powder diffraction: At room temperature using (XRD-6000, Shimadzu-Japan) was employed for obtaining x-ray powder diffraction patterns samples of SL, SC and the OSLM. Anode was Cu and graphite monochromator, operated at a voltage of 40 kV and 30 mA current. Samples were analyzed in the 2θ angle range of 5°–70° and the process parameters were set as: scan step size of 0.02° (2θ), and scan step time of 0.5 degree/min.

Fourier transform infrared spectroscopy: Grounded powder samples of SL, SC and the OSLM were mixed thoroughly with KBr at 1: 5 ratios for developing an infrared transparent matrix, respectively. A hydraulic press was employed for KBr discs preparation at a pressure of 5 tons for 5 min and then (FTIR-600 FTIR Spectrometer, Main FTOS Biotech Engineering Management Co. Ltd-UK) was employed for samples scanning at a resolution of 4 cm⁻¹, from 4000 to 400 cm⁻¹.

In vitro dissolution and release kinetics: Microparticles samples each equivalent to 30 mg SL were placed in the dissolution vessels USP type II dissolution test apparatus (TDT-06P-ELECTROLAB-India) each containing 1000 ml of phosphate buffer pH 7.4 maintained at 37 ± 0.5 °C/stirred at 100 rpm and the withdrawn samples were replaced with equal quantity of fresh dissolution medium to ensure sink condition. The samples were analyzed for SL after filtration through a 0.45 μm filter membrane by UV spectroscopy (SPECORD[®] 40-Analytik Jena AG-Germany) at λ_{max} 238nm^[15]. The release data were fitted according to five kinetic model-dependent equations in order to find the one with the best fit using DDSolver software (Zhang, China)^[16]:

$$R = k_0 t \quad (4)$$

$$\text{Log UR} = \frac{k_1 t}{2.303} \quad (5)$$

$$R = k_H \sqrt{t} \quad (6)$$

$$(\text{UR})^{1/3} = k_{HC} t \quad (7)$$

$$\text{Log R} = \text{Log } k_{KP} + n \text{ Log } t \quad (8)$$

where R and UR are the released and unreleased percentages, respectively, at time (t): k_0 , k_1 , k_H , k_{HC} and k_{KP} are the rate constant of zero-order, first-order, Higuchi matrix, Hixson-Crowell and Korsmeyer-Peppas model respectively.

III. Results and Discussions

Formulation optimization: Study optimization was conducted by response surface methodology and the results are shown in table 2 where the experimental designs and the corresponding responses are fixed. Polynomial models were employed for fitting the experimental designs responses and an analysis of variance (ANOVA) test for their significance estimation as shown in table 3, where Y_1 , Y_2 , Y_3 and Y_4 fit a first-order, two factor interaction and quadratic model [17].

Run	X ₁ ; CS %	X ₂ ; AA %	X ₃ ; GA %	Y ₁ ; AOR θ	Y ₂ ; GSD μm	Y ₃ ; FPF %	Y ₄ ; MMAD μm
1	2.80	1.95	0.33	32.3	9.36	46.085	5.282
2	2.80	1.95	0.33	33.4	9.72	47.191	5.299
3	2.80	1.95	0.45	37.6	7.37	32.224	6.894
4	1.60	1.00	0.40	44.5	8.17	28.191	7.555
5	4.82	1.95	0.33	41.3	14.43	28.536	6.390
6	2.80	0.35	0.33	38.5	22.08	5.308	10.26
7	0.78	1.95	0.33	32.3	12.86	42.802	5.296
8	2.80	3.55	0.33	34.5	6.07	52.992	5.046
9	2.80	1.95	0.00	43.0	2.17	55.747	4.081
10	4.00	2.90	0.25	35.2	3.83	46.056	5.428
11	2.80	1.95	0.33	33.2	9.75	46.804	5.255
12	2.80	1.95	0.33	32.2	9.67	46.387	5.242
13	1.60	2.90	0.40	31.5	7.07	47.114	5.310
14	4.00	1.00	0.25	44.1	10.09	32.733	6.623
15	1.60	2.90	0.25	30.4	4.94	40.981	5.497
16	4.00	2.90	0.40	33.3	11.35	43.473	5.975
17	4.00	1.00	0.40	40.3	12.77	19.265	7.683
18	2.80	2.90	0.33	33.0	9.04	46.549	5.259
19	2.80	2.90	0.33	35.3	8.94	46.956	5.268
20	1.60	1.00	0.25	42.3	5.45	41.778	5.230

Here below are models that have been established from the CCD runs:

$$Y_1 = 55.91 - 1.73x_1 - 13.13x_2 - 34.74x_3 + 0.99x_1x_2 - 11.82x_2x_3 + 3.18x_1x_3 + 0.87x_1^2 + 1.53x_2^2 + 99.89x_3^2 \quad (9)$$

$$Y_2 = 18.26 - 2.75x_1 - 7.23x_2 + 3.3x_3 - 0.67x_1x_2 + 7.08x_2x_3 + 6.28x_1x_3 + 0.47x_1^2 + 1.16x_2^2 - 35.43x_3^2 \quad (10)$$

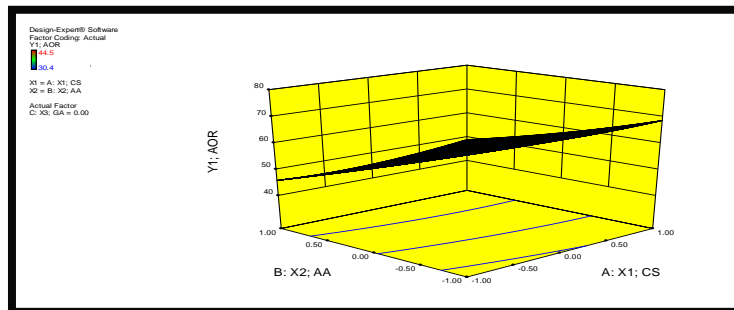
$$Y_3 = 39.45 + 8.78x_1 + 9.64x_2 - 79.39x_3 + 2.13x_1x_2 - 12.58x_2x_3 + 56.03x_1x_3 - 2.02x_1^2 - 6.12x_2^2 - 77.79x_3^2 \quad (11)$$

$$Y_4 = 4.52 + 0.21x_1 - 2.24x_2 + 12.85x_3 - 0.1x_1x_2 - 0.72x_2x_3 - 5.64x_1x_3 + 0.082x_1^2 + 0.86x_2^2 + 12x_3^2 \quad (12)$$

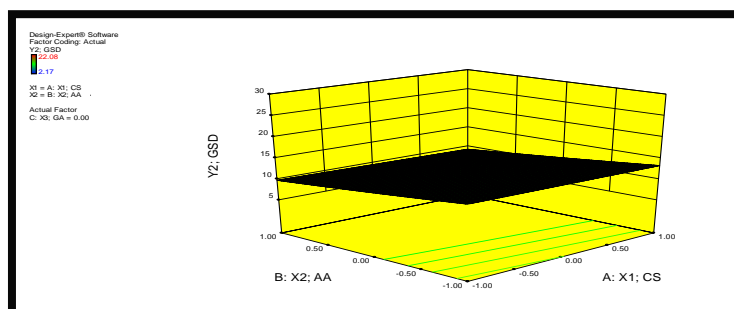
Coefficients exist within the polynomial equation represent the intercept, first order main effect, interaction terms and higher order effects. Associated response p values for Y_1 , Y_2 , Y_3 and Y_4 results for the factor effects are showed in table 3. The relative influence for each response factor is indicated by the sign and magnitude of the main effect where a synergistic effect when the sign is positive, whereas an antagonistic effect when the sign is negative. Response surface methodology 3-D response surface plot are shown in figure 1.

Source of Variation	ANOVA results				p Summary	
	Sum of Square	DF	Mean of Square	F Value	Value	Significant
AOR (θ)						
Quadratic Model	307.08	9	34.12	4.257	0.0126	Significant
X ₁ - CS	25.403	1	25.403	3.169	0.0898	
X ₂ - AA	155.757	1	155.757	19.439	0.0010	
X ₃ - GA	9.208	1	9.208	1.153	0.2758	
GSD (μm)						
Quadratic Model	210.89	9	23.429	2.948	0.0179	Significant
X ₁ - CS	12.702	1	12.702	1.600	0.1371	
X ₂ - AA	73.535	1	73.535	9.257	0.0046	
X ₃ - GA	31.745	1	31.745	3.997	0.0348	
FPF (%)						
Quadratic Model	2556.13	9	284.015	6.489	0.0015	Significant

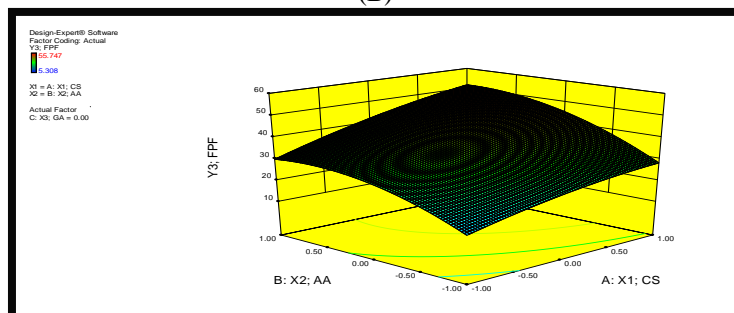
X_1 – CS	100.587	1	100.587	2.299	0.1073	
X_2 – AA	1113.799	1	1389.770	31.770	0.00008	
X_3 – GA	243.548	1	243.548	5.569	0.0229	
MMAD (μm)						
Quadratic Model	30.84	9	3.43	8.444	0.0013	Significant
X_1 – CS	1.16	1	1.16	2.845	0.1248	
X_2 – AA	13.76	1	13.76	33.906	0.0002	
X_3 – GA	5.306	1	5.306	13.074	0.0048	



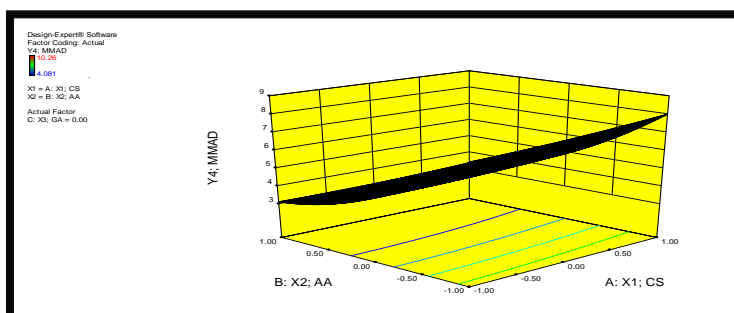
(A)



(B)



(C)



(D)

Figure 1: Response surface plots for the CS (X_1), AA (X_2) and GA (X_3) on the AOR (Y_1)-A, GSD (Y_2)-B, FPF (Y_3)-C and MMAD (Y_4)-D

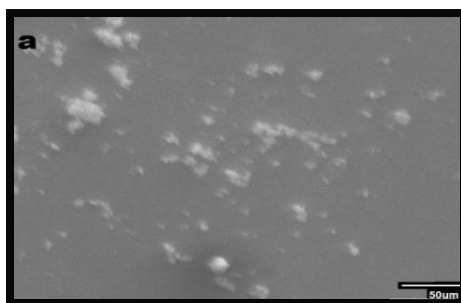
Angle of repose (AOR) (θ) parameter measurement is employed in powder flow determination; factor X_2 F values are higher than X_1 (Table 3), i.e. X_2 more significantly affected the response variable. Figure 1 (A) shows that θ increases upon CS increment whereas the reverse happened with AA. Equation 9 shows that both CS and AA reduced the θ by the negative coefficients for X_1 and X_2 . Figure 1 (B) shows the CS and AA combined effect had on the geometrical standard diameter (GSD) (Y_2).

Figure 1 (C) reveals the CS and AA concentrations, X_1 and X_2 respectively response surface plot for fine particle fraction (FPF) (Y_3) and table 3 shows that X_2 F values are higher than X_1 , i.e. X_2 more significantly affected the response variable. The existence of CS yielded positive X_1 as well as AA yielded positive X_2 . The FPF improved upon CS increment, although larger amounts will decrease the aerosolization performance due to some degree of CS microparticles aggregation and a greater polymer amount in the same volume of jelly liquid droplets passing through a sieve screen [18]. The existence of acetic acid will aid in the aerodynamic particle size distribution and the powder respirability improvement which was determined by the peculiar shriveled shape and microparticles composition density [19]. Finally, figure 1 (D) shows the effect of X_1 and X_2 on the microparticles mass median aerodynamic diameter (MMAD) (Y_4) response surface plot and table 3 shows that X_2 F values are higher than X_1 , i.e. X_2 more significantly affected the response variable. The formulation excipients combination enhances the powder aerodynamic properties and yields mainly AA, dry powder particle size and dispersion mechanism used to aerosolize the powder [20].

In vitro optimization of dry powder microparticles: Formulation optimization based on minimizing AOR (Y_1), GSD (Y_2) and FPF (Y_3), while maximizing MMAD (Y_4). Applying desirability function method based on all of the investigated formulation variables in order to predict the optimum formulation variables range [21]. In order to prove the validity of the calculated optimal factors and predicted responses, a new SL formula was prepared using the optimum formulation and the responses were observed, table 4. The overall desirability was 0.956, where the prediction model was 103.272%, 97.325%, 102.389% and 105.393% for the AOR, GSD, FPF and MMAD, respectively and hence it is desirable.

Table 4: Spironolactone dry powder microparticles observed and predicted values			
Factor	Optimized Level		
X_1 ; CS (% w/v)	2.435		
X_2 ; AA (% w/v)	2.253		
X_3 ; GA (% w/v)	0.051		
Desirability	0.956		
Response	Expected	Observed	Residual
Y_1 : angle of repose (AOR, θ)	38.037	38.706	0.669
Y_2 : the geometric standard diameter (GSD, μm)	3.9397	3.7763	-0.163
Y_3 : fine particle fraction (FPF, %)	58.882	59.410	0.528
Y_4 : the mass media aerodynamic diameter (MMAD, μm)	2.2925	2.3808	0.088

Scanning electron microscopy: The electronic images in figure 2 shown that SL powder particles are characterized by a large prismatic crystal shape [22], CS particles are large, irregular and with smooth surfaces, whereas the OSLM are within the acceptable inhaling range and with rough surfaces due to the cross-linked CS with GA [23].



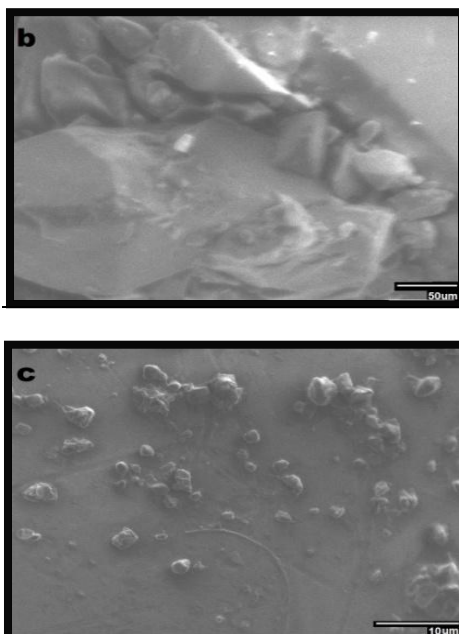
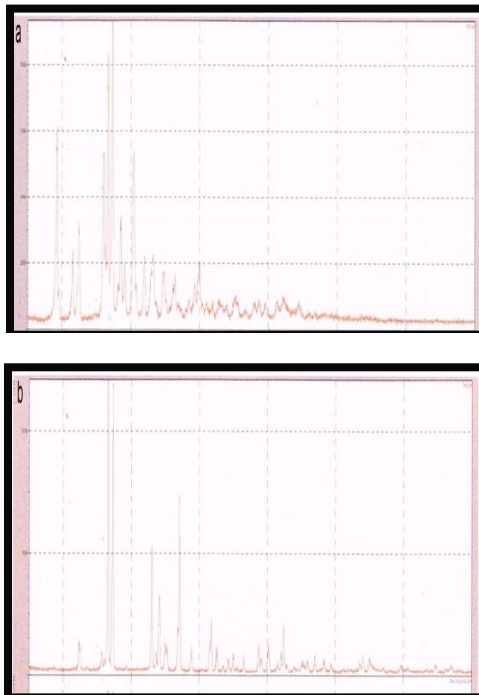


Figure 2: Scanning electron micrographs of (a) SL, (b) CS and (c) OSLM

XRDP: The crystalline nature was found by employing the XRD, which figure 3 shows that SL was crystalline as it was revealed by its numerous peaks at 20 of 9.18, 16.66, 17.3, and 20.28^[24]. The semicrystalline nature of pure CS characterized by 11 and 20 peaks, whereas the OSLM peaks at 22 and 42 indicate CS minor transformation into amorphous nature due to the cross-linked CS with GA and the SL low intense peaks appear on the same diffraction spectra indicate some amorphous changes in drug crystalline nature due to low drug amount exist per cross-linked powder^[25].



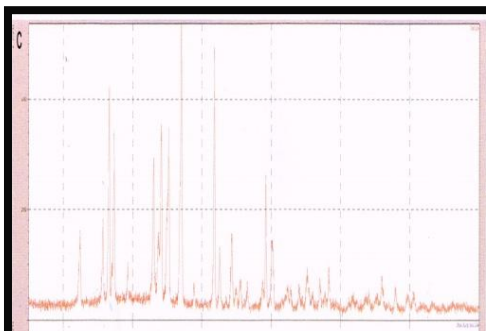


Figure 3: X-ray diffraction patterns of (a) SL, (b) CS and (c) OSLM

FTIR: The FTIR spectra of the samples are shown in figure 4, where SL spectrum has peaks at 1618 cm^{-1} ($\text{C}=\text{C}$ stretching of α, β -unsaturated ring), 1678 cm^{-1} ($\text{C}=\text{O}$ stretching of α, β -unsaturated ring), 1768 cm^{-1} ($\text{C}=\text{O}$ stretching of thioacetyl group) and 2951 cm^{-1} ($\text{C}-\text{H}$ stretching) [26]. Pure CS absorption bands at 2947 cm^{-1} ($-\text{OH}$ stretching), 1383 cm^{-1} ($\text{CH}_2=\text{CH}_2$ bending), 1417 cm^{-1} ($-\text{CH}_3$ bending) and 1063 cm^{-1} ($\text{C}-\text{O}$ stretching vibration of the ring $\text{C}-\text{O}-\text{H}$, $\text{C}-\text{O}-\text{C}$ and CH_2OH), whereas the OSLM absorption bands at 2841 cm^{-1} and 1421 cm^{-1} (aliphatic $\text{C}-\text{H}$ stretching) and the most prominent is 1610 cm^{-1} ($\text{C}=\text{N}$ Schiff base stretching) [27]. The 1768 cm^{-1} ($\text{C}=\text{O}$ stretching of thioacetyl group) of SL although shown to become very small in the OSLM spectra which indicate no physicochemical interactions between the drug and the carrier.

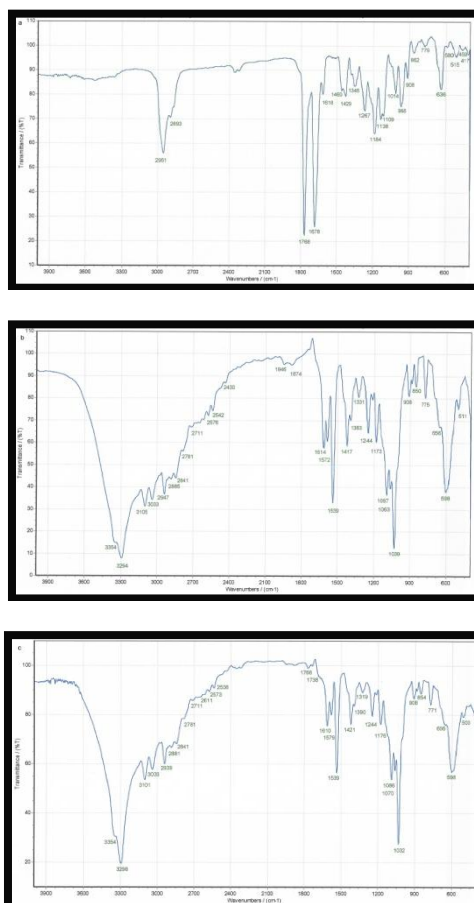


Figure 4: FTIR spectra of (a) SL, (b) CS and (c) OSLM

In vitro release kinetic model and mechanism of SL from the optimized microparticles: In comparison with crystalline SL, the cumulative percentage of SL released from the OSLM is depicted in figure 5, where the former release was less than 40% within 6 hours, because the rate of dissolution is directly proportional to the drug particle surface area and nature, i.e. in the case of pure SL is large and crystalline respectively [28], whereas the latter release was approximately 100%, biphasic release pattern was a characteristic feature of the OSLM release profile and was highest, gradual and more sustained within the 6 hours of release. This is because the

cross-linked CS releases its content rapidly comes from the instantaneous swelling at higher pH, where the first 30 min burst of release is due to the untrapped drug adheres to the microparticles surfaces after the initial rapid hydration and swelling, whereas the latter slow release is due to the drug residual amount depletion in the microparticles and the concentration gradient build-up in the dissolution medium with time [29].

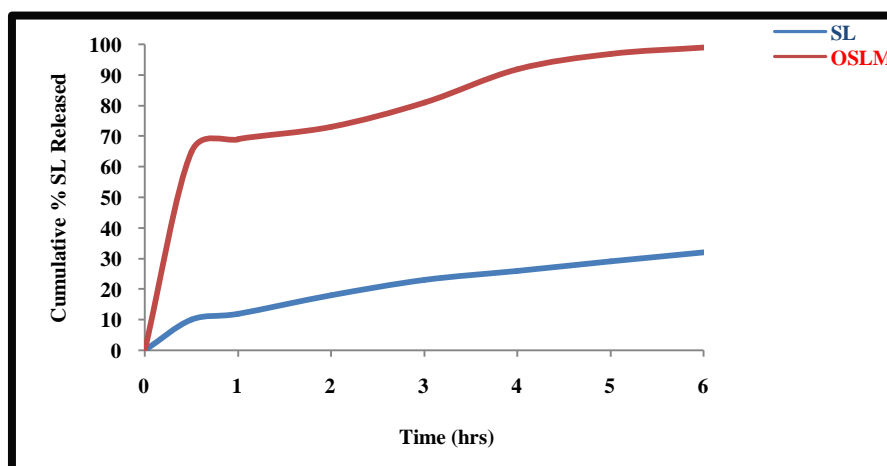


Figure 5: Cumulative percentage of SL released from drug suspension and the OSLM in phosphate buffer of pH 7.4

Table 5 shows the OSLM data that indicate Korsmeyer-Peppas model of release is of best fitness and the release mechanism was Fickian diffusion as the release exponent is ($n \leq 0.45$) [30].

Table 5: OSLM release kinetic data

Zero-Order Model		First-Order Model		Higuchi-Matrix Model		Hixson-Crowell Model		Korsmeyer-Peppas Model		
R ²	K ₀ (%h ⁻¹)	R ²	K ₁ (h ⁻¹)	R ²	K _H (%h ^{-1/2})	R ²	K _{HC} (%h ⁻¹)	R ²	n	K _{KP} (%h ⁻ⁿ)
0.8003	21.233	0.9493	1.23	0.9228	46.6	0.9147	0.237	0.9937	0.192	69.125

IV. Conclusions

Spironolactone loaded CS-based dry powder was prepared by employing the sieving method utilizing cross-linked CS with GA as the carrier, where an optimized pulmonary sustained-release delivery system can be achieved after studying formulation variables influence on the responses of prime importance to the development of DPI. The results obtained from this study imply the potential of sieving method in the preparation of DPI for delivering drugs to the deep lung.

Acknowledgements

The authors' deepest gratitude goes to the State Company for Drug Industries and Medical Appliances (SDI) (Samarra / Iraq) for providing the gift sample of spironolactone and many thanks to the Baghdad College of Pharmacy for permission to perform this work in the research laboratory.

References

- [1] Hoepfer MM, Gibbs SR. The Changing Landscape of Pulmonary Arterial Hypertension and Implications for Patient Care. *European Respiratory Review* 2014; 23(134): 450 – 457.
- [2] Lai YC, Potoka KC, Champion HC, Mora AL, Gladwin MT. Pulmonary Arterial Hypertension: The Clinical Syndrome. *Circulation Research* 2014; 115: 115 – 130.
- [3] Ryan JJ, Archer SL. The Right Ventricle in Pulmonary Arterial Hypertension: Disorders of Metabolism, Angiogenesis and Adrenergic Signaling in Right Ventricular Failure. *Circulation Research* 2014; 115: 176 – 188.
- [4] Maron BA, Leopold JA. The Role of the Renin-Angiotensin-Aldosterone System in the Pathobiology of Pulmonary Arterial Hypertension (2013 Grover Conference series). *Pulmonary Circulation* 2014; 4(2): 200 – 210.
- [5] Elinoff JM, Rame JE, Forfia PR, Hall MK, Sun J, Gharib AM, Abd-Elmoniem K, Graninger G, Harper B, Danner RL, Solomon MA. A Pilot Study of the Effect of Spironolactone Therapy on Exercise Capacity and Endothelial Dysfunction in Pulmonary Arterial Hypertension: Study Protocol for a Randomized Controlled Trial. *Trial Journal* 2013; 14: 2 – 16.
- [6] Ruge CA, Kirch J, Lehr C-M. Pulmonary Drug Delivery: From Generating Aerosols to Overcoming Biological Barriers—Therapeutic Possibilities and Technological Challenges. *The Lancet Respiratory Medicine* 2013; 1(5): 402 – 413.
- [7] Wu Q-X, Lin D-Q, Yao S-J. Design of Chitosan and Its Water Soluble Derivatives-Based Drug Carriers with Polyelectrolyte Complexes. *Marine Drugs* 2014; 12(12): 6236 – 6253.
- [8] Langguth P, Hanafy A, Frenzel D, Grenier P, Nhamias A, Ohlig T, Vergnault G, Spahn-Langguth H. Nanosuspension Formulations for Low-Soluble Drugs: Pharmacokinetic Evaluation Using Spironolactone as Model Compound. *Drug Development and Industrial Pharmacy* 2005; 31(3): 319 – 329.

- [9] Kadir MF, Alam MR, Rahman AB, Jhanker YM, Shams T, Khan RI. Study of Binary and Ternary Solid Dispersion of Spironolactone Prepared By Co-Precipitation Method for the Enhancement of Oral Bioavailability. *Journal of Applied Pharmaceutical Science* 2012; 2(10): 117 – 122.
- [10] Singh DJ, Lohade AA, Parmar JJ, Hegde DD, Soni P, Samad A, Menon MD. Development of Chitosan-Based Dry Powder Inhalation System of Cisplatin for Lung Cancer. *Indian Journal of Pharmaceutical Sciences* 2012; 74(6): 521 – 526.
- [11] Agnihotri SA, Aminabhavi TM. Controlled Release of Clozapine Through Chitosan Microparticles Prepared by a Novel Method. *Journal of Controlled Release* 2004; 96(2): 245 - 259.
- [12] Pilicheva B, Katsarov B, Kassarova M. Flowability Evaluation of Dry Powder Inhalation Formulations Intended for Nasal Delivery of Betahistine Dihydrochloride. *SMU Medical Journal* 2015; 2(1): 77 – 90.
- [13] Abbas Z, Marihal S. Gellan Gum-Based Mucoadhesive Microspheres of Almotriptan for Nasal Administration: Formulation Optimization using Factorial Design, Characterization, and in vitro Evaluation. *Journal of Pharmacy and BioAllied Sciences* 2014; 6(4): 267 – 277.
- [14] Mishra M, Mishra B. Mucoadhesive Microparticles as Potential Carriers in Inhalation Delivery of Doxycycline Hyclate: A Comparative Study. *Acta Pharmaceutica Sinica B* 2012; 2(5): 518 – 526.
- [15] Yassin AE, Alanazi F, EL-Badry M, Alsarra IA. Preparation and Characterization of Spironolactone-Loaded Gelucire Microparticles Using Spray-Drying Technique. *Drug Development and Industrial Pharmacy* 2008; 35(3): 297 – 304.
- [16] Zhang Y, Huo M, Zhou J, Zou A, Li W, Yao C, Xie S. DDSolver: An Add-In Program for Modeling and Comparison of Drug Dissolution Profiles. *The AAPS Journal* 2010; 12(3): 263–271.
- [17] Khodadoust S, Hadjmohammadi M. Determination of Nmethylcarbamateinsecticides in Water Samples Using Dispersive Liquid–Liquid Microextraction and HPLC with the Aid of Experimental Design and Desirability Function. *Analytica Chimica Acta* 2011; 699(1): 113 – 119.
- [18] Kundawala AJ, Patel VA, Patel HV, Choudhary A. Influence of Formulation Components on Aerosolization Properties of Isoniazid Loaded Chitosan Microspheres. *International Journal of Pharmaceutical Sciences and Drug Research* 2011; 3(4): 297 – 302.
- [19] Sonvico F, Rossi A, Colombo G, Colombo P. Pure Insulin Highly Respirable Powders for Inhalation. *European Journal of Pharmaceutical Sciences* 2014; 51: 110 – 117.
- [20] Zhang Y, Wang X, Lin X, Liu X, Tian B, Tang X. High Azithromycin Loading Powders for Inhalation and their In Vivo Evaluation in Rats. *International Journal of Pharmaceutics* 2010; 395 (1 – 2): 205 – 214.
- [21] Seville PC, Learoyd TP, Li HY, Williamson IJ, Birchall JC. Amino Acid-Modified Spray-Dried Powders with Enhanced Aerosolisation Properties for Pulmonary Drug Delivery. *Powder Technology* 2007; 178 (1): 40 – 50.
- [22] Brandao FC, Tagiari MP, Silva MAS, Berti LF, Stulzer HK. Structure of Chemical Compounds, Methods of Analysis and Process Control: Physical – Chemical Characterization and Quality Control of Spironolactone Raw Material Samples. *Pharmaceutical Chemistry Journal* 2008; 42(6): 368 – 376.
- [23] Ostrowska-Czubenko J, Gierszewska M, Pieróg M. pH-Responsive Hydrogel Membranes Based on Modified Chitosan: Water Transport and Kinetics of Swelling. *Journal of Polymer Research* 2015; 22(153): 1 – 12.
- [24] Paul PK, Dey LR, Shahriar M, Dewan I, Islam SMA. Comparative In Vitro Dissolution Study of Spironolactone from Binary and Tertiary Solid Dispersion: Model Dependent and Independent Approaches. *Journal of Drug Delivery and Therapeutic* 2012; 2(4): 73 – 80.
- [25] Acharyulu SR, Gomathi T, Sudha PN. Physico-Chemical Characterization of Cross-Linked Chitosan-Polyacrylonitrile Polymer Blends. *Der Pharmacia Lettre* 2013; 5 (2): 354 – 363.
- [26] Akbari J, Saeedi M, Morteza-Semnani K, Kelidari HR, Moghanlou FS, Zareh G, Rostamkalaei S. The Effect of Tween 20, 60, and 80 on Dissolution Behavior of Sprionolactone in Solid Dispersions Prepared by PEG 6000. *Advanced Pharmaceutical Bulletin* 2015; 5(1): 1 – 7.
- [27] Ramachandran S, Nandhakumar S, Dhanaraju MD. Formulation and Characterization of Glutaraldehyde Cross-Linked Chitosan Biodegradable Microspheres Loaded with Famotidine. *Tropical Journal of Pharmaceutical Research* 2011; 10 (3): 309 – 316.
- [28] Shamma RN, Aburahma MH. Follicular Delivery of Spironolactone via Nanostructured Lipid Carriers for Management of Alopecia. *International Journal of Nanomedicine* 2014; 9: 5449 – 5460.
- [29] Ofokansi KC, Kenechukwu FC, Isah AB, Okigbo EL. Formulation and Evaluation of Glutaraldehyde-Crosslinked Chitosan Microparticles for the Delivery of Ibuprofen. *Tropical Journal of Pharmaceutical Research* February 2013; 12 (1): 19 - 25.
- [30] Chime SA, Onunkwo GC, Onyishi II. Kinetics and Mechanisms of Drug Release from Swellable and Non Swellable Matrices: A Review. *Research Journal of Pharmaceutical, Biological and Chemical Sciences* 2013; 4(2): 97 – 103.